Proceedings of ASME Turbo Expo 2011
GT2011
June 6-10, 2011, Vancouver, British Columbia, Canada

GT2011-46237

NUMERICAL OPTIMIZATION OF A STEAM TURBINE CONTROL STAGE BY FLOWPATH PROFILING USING EVOLUTIONARY ALGORITHM

Nils Moser
Power Engineering
Laboratory of Turbomachinery
Helmut Schmidt University
University of the Federal
Armed Forces Hamburg
Holstenhofweg 85,
D-22043 Hamburg, Germany
E-mail: moser@hsu-hh.de

René Volkert
Calculation and Development
MAN Diesel & Turbo SE
Hermann-Blohm-Strasse 5,
D-20457 Hamburg, Germany
E-mail: rene.volkert@man.eu

Franz Joos
Power Engineering
Laboratory of Turbomachinery
Helmut Schmidt University
University of the Federal
Armed Forces Hamburg
Holstenhofweg 85,
D-22043 Hamburg, Germany
E-mail: joos@hsu-hh.de

ABSTRACT

The subject of this paper is the optimization of a steam turbine impulse wheel control stage by flowpath profiling of the shroud. The investigated control stage is derived from an existing industrial steam turbine design. The shroud contour is varied in radial direction within specified restrictions by an evolutionary algorithm. The algorithm is directly connected to a mesh generator and a CFD solver.

The optimization goal is the reduction of the total pressure loss over the guide vanes. The geometry of the rotor blade has been retained unchanged within the presented investigations. The flow field of the varied stage is compared with the baseline geometry. The optimum candidates are further investigated with CFD simulations for different operating point scenarios.

Numerical results show that the axisymetric flowpath profiling of the shroud has a considerable effect on the loss behavior of the whole stage over a wide range of pressure ratios. Due to flowpath profiling the boundary layer in the nozzle is significantly affected which results in a more uniformly shaped exit flow angle profile over the nozzle span and a significant reduction of the global secondary flow effects in the guide vanes. Both observations have a positive influence on the flow conditions to the subsequent rotor blade.

NOMENCLATURE

α_1	exit flow angle at guide vane outlet
β_s	stagger angle
c_0	velocity at guide vane inlet
c_1	velocity at guide vane outlet
c_2	velocity at rotor blade outlet
c_p	specific heat coefficient at constant pressure
c_s	nozzle chord
η_i	stage efficiency coefficient
η_{GV}	guide vane efficiency coefficient
Δh_s	isentropic enthalpy difference
κ	isentropic coefficient of air
$\dot{m}$	mass flow rate
P	power output
p_0	static pressure at guide vane inlet (mean value)
p_1	static pressure at guide vane outlet (mean value)
$p_{t,0}$	total pressure at guide vane inlet (mean value)
$p_{t,1}$	total pressure at guide vane outlet (mean value)
$p_{t,2}$	total pressure at rotor outlet (mean value)
π	pressure ratio ($p_{t,0}$/ $p_{t,2}$)
r_K	reaction (h_2/h)
R_s	shroud radius
$R_{s,max}$	maximum shroud radius
$R_{s,min}$	minimum shroud radius
R_h	hub radius
T_0	temperature at guide vane inlet
ζ_{pt}	total pressure loss

INTRODUCTION

Secondary losses, in addition to profile losses, are one of the most important loss mechanisms in turbo machines. Their influence emerges in particular at blade profiles with high aerodynamic loads, high pressure ratio, high flow velocity and low aspect ratio. Secondary losses can constitute up to 30% of the overall loss. The effect of secondary flows has been intensively investigated by Langston [1], Sieverding [2] and Gregory-Smith [3]. Dejc and Zarjankin have shown that secondary losses and boundary layer effects can be reduced by an axisymetric end wall contour [4]. They used a cubic function to define the end wall contour. Moustapha and Williamson [5] investigated radial constrictions in the meridian plane. They asserted that a streamwise downward constriction exhibits a lower loss than a linear one. Rose [6] achieved a significant influence of the static pressure at the profiled wall by a three-dimensional contouring of a high pressure gas turbine. Schnaus and Fottner [7] as well as Duden et al. [8] investigated axisymetrically contoured end walls of rotor blades. They observed a reduction in the variance of the exit flow angle. A decrease of the losses was not observed. In combination with thickening and sweep of the blade profile a significant reduction of the losses and the variance of the exit flow angle were achieved. Harvey et al. [9] examined a 3D hub contour of a turbine. The contour was described with a deviation from the reference contour at six axial positions in circumferential direction by a Fourier function. The static pressure distribution at the hub surface and the exit flow angle variation were selected as optimization target. Harvey et al. asserted that the passage vortex and the overall losses were reduced by the 3D profiled hub. Furthermore, they discovered a new vortex near the hub. Experiments by Hartland et al. [10] validated these results. Eymann et al. [11] experimentally investigated an axisymmetric end wall contour simultaneous with a blade profile optimization in the first stage of a gas turbine. They affirmed that the vortex system behind the first guide vane was dislocated near the end walls. Additionally, Eymann observed a reduction of the passage and the trailing edge vortex as a result of his optimization.

The literature survey obviously shows that most of the optimization tasks were done in the gas turbine sector. The presented work is meant to be a starting point for similar efforts in the steam turbine sector.

GEOMETRY RESTRICTION

The control stage investigated here is derived from an impulse wheel design of an existing industrial steam turbine. Due to the manufacturing process and the resultant costs of the steam turbine guide vanes for control stages the shroud contour has to be axisymmetric. Furthermore Dejc [16] pointed out that only an asymmetric contraction of the flowpath fulfills the requirement of secondary loss reduction and small radial pressure gradients respectively. The shroud contour is defined by an equidistant distribution of nine points which describes a b-spline as shown in Fig. 1.

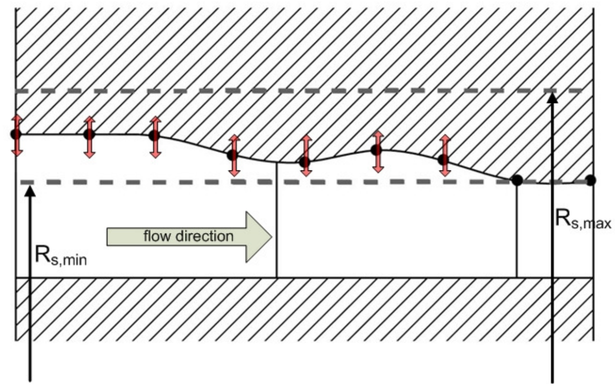

Figure 1. ILLUSTRATION OF GEOMETRY RESTRICTION.

Seven of these points are varied in radial direction within the following limits of R_s:

$$R_{s,min} = R_h + 0.25 * c_s \leq R_s \leq R_h + 0.5 * c_s = R_{s,max} \quad (1)$$

To avoid flow disturbances at the inlet and outlet of the guide vane channel the radial shroud contour gradient is set to zero. Consequently there is no shroud curvature at the inlet and outlet. Since the subsequent rotor blade configuration retains unchanged the cross section of the vane outlet is fixed for all geometry variants.

EVOLUTIONARY ALGORITHM

The optimization of the shroud contour is a complex multidimensional problem. The optimization parameters are the radial positions of the seven flexible points, which describe the contoured shroud. Due to seven degrees of freedom a simple analytic solution is not suitable. In order to achieve a systematic optimization of the shroud profile an evolutionary algorithm has been used. The main loss mechanism in guide vanes is the total pressure loss due to secondary flow regimes. Hence only the total pressure loss of the guide vane is selected as fitness function for the evolutionary algorithm. It is evaluated as shown in Eqn. (2). In a first step no additional constrains to the algorithm in terms of mass flow deviation or exit angle range are implemented.

$$\zeta_{Pt} = 1 - \frac{1 - \left(\frac{p_1}{p_{t,1}}\right)^{\frac{\kappa-1}{\kappa}}}{1 - \left(\frac{p_1}{p_{t,0}}\right)^{\frac{\kappa-1}{\kappa}}} \quad (2)$$

An evolutionary optimization is based on the technique of adaption and evolution as shown by Rechenberg [12] and Weicker [13]. The workflow of the evolutionary algorithm is shown in Fig. 2. The creation method of the child individual is randomly selected. Through this selection the algorithm becomes more flexible. After gaining the geometry information for the child individual the pressure loss is evaluated. Due to the influence of the flowpath profiling on the secondary flow

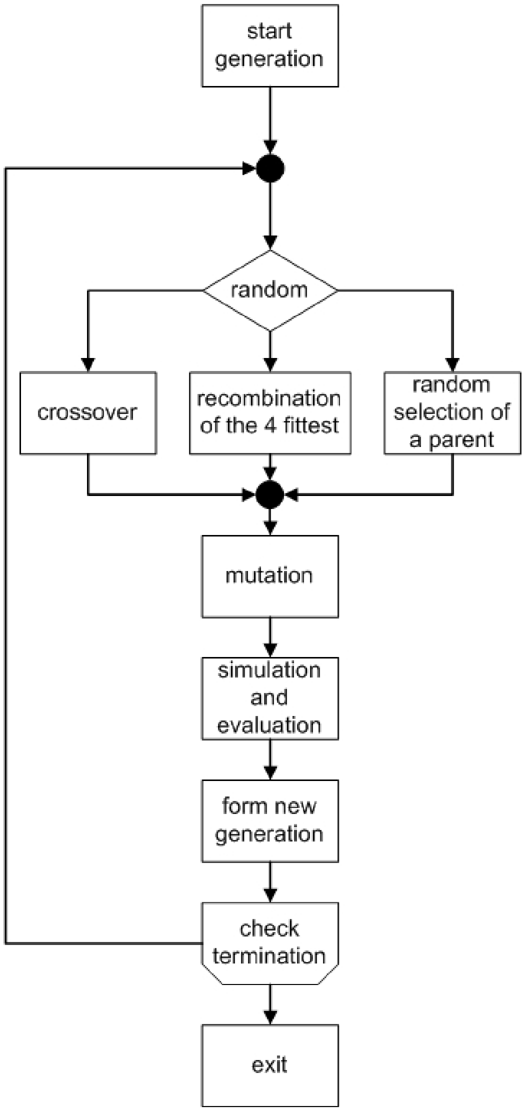

Figure 2. WORKFLOW OF EVOLUTIONARY ALGORITHM.

phenomena every single individual must be simulated by means of 3D-CFD. Therefore the evolutionary algorithm is directly connected to a commercial mesh generator and CFD solver. ANSYS CFX 12.0 is used as CFD solver. The mesh generator creates the three-dimensional numerical model and hands it over to the CFD solver which simulates and evaluates every single child individual. The numerical mesh was generated by means of a H-grid topology with additional O-grid to fulfill the simulation requirements for boundary layers. Finally a mesh of about one million control volumes was created for the guide vane geometry. With this grid resolution mesh independent numerical results were achieved for all geometries. The Y+ value for all simulations is around two. Figures 3 and 4 show the topology and the density of the mesh. The shear stress transport model is used as turbulence model. The convergence

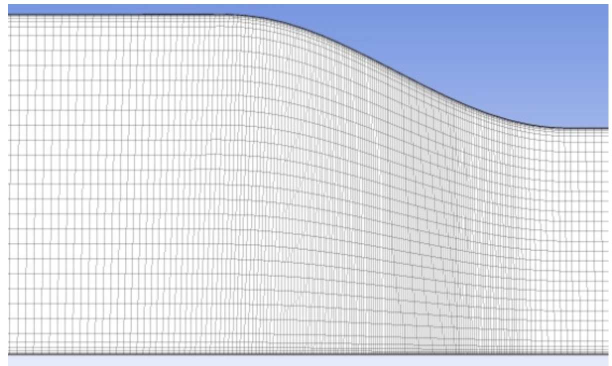
Figure 3. MESH CHANNEL.

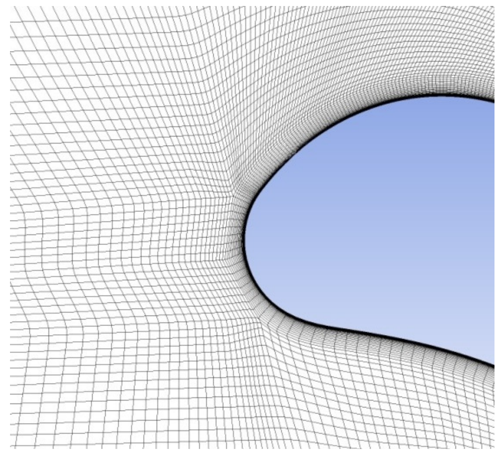
Figure 4. MESH DETAILS AT LEADING EDGE.

criteria is an overall residual below 10^{-5}. The optimization algorithm is based on Darwin's principal "survival of the fittest". This implies that only the fittest individual of the parent generation and the child individuals are transferred to the next generation. The optimum candidates are further investigated with and without the interaction to the subsequent rotor blade. A (μ+λ)-strategy has been selected as the evolutionary strategy. This means that from μ parental individuals λ child individuals are generated and the μ fittest individuals are passed to the next generation. Parental individuals can be transferred to the next generation, too.

One problem of this strategy is that the algorithm tends to hang up on a local optimum but on the other side the algorithm is quite fast and robust. For the creation of the child individuals three different mechanisms are required:

- simple mutation
- recombination of the four fittest
- crossover

Detailed information about the evolutionary algorithm can be gained at [14].

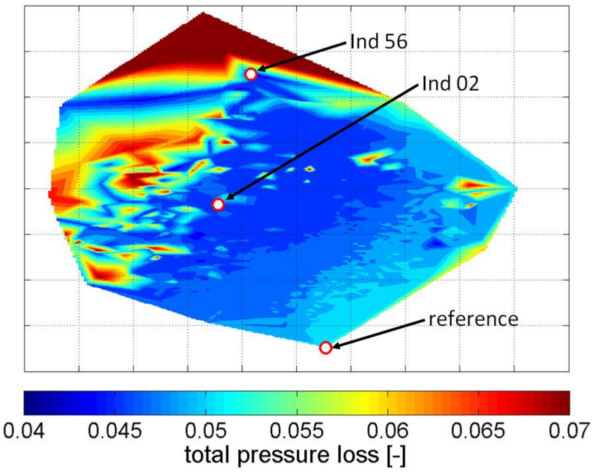

Figure 5. MULTIDIMENSIONAL SCALING.

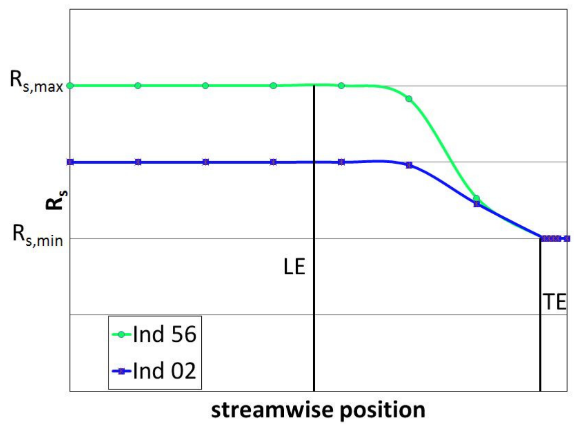

Figure 6. ILLUSTRATION OF THE INVESTIGATED CONTOURS.

RESULTS

In the first step the operating point is kept constant during optimization. Only the guide vane geometry is simulated. The optimum candidate is investigated further with CFD simulations for different operating point scenarios and with the rotor blade. The design pressure ratio over the nozzle is $\pi = 2$. Air is the chosen fluid because in a further step the result will be compared with measurements of an air turbine test rig. The original shroud contour with a constant shroud radius $R_s = R_{s,min}$ is used as the reference geometry.

In order to visualize properly the target function of the shroud variation a multidimensional scaling is used to project the eight-dimensional space on a three-dimensional space. The transformation scheme is given in Eqn. (3). Individuals which are close to each other in the eight-dimensional space are also close in the three-dimensional space. As goodness-of-fit criterion the minimum of the squared stress normalized with the sum of fourth powers of the dissimilarities is used. Further

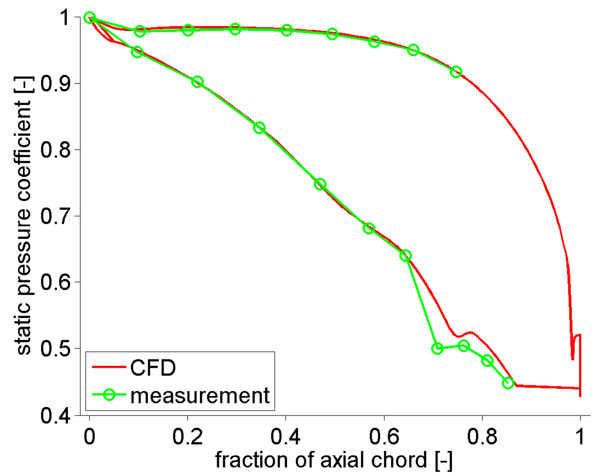

Figure 7. COMPARISON CFD / MEASUREMENT.

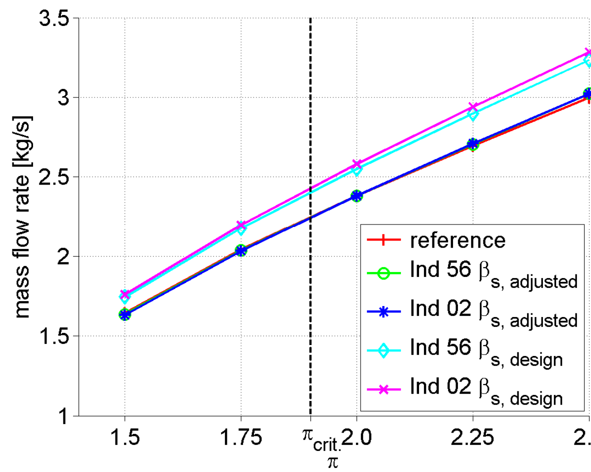

Figure 8. MASSFLOW.

information can be found at Seber [15]. Figure 5 shows the multidimensional scaling map of the total pressure loss ζ_{Pt} as the target function over the transformed coordinates R_1^* and R_2^*. The map was generated using the information of over 2500 individuals.

$$\begin{pmatrix} R_{S,1} \\ \vdots \\ R_{S,7} \\ \zeta_{Pt} \end{pmatrix}_j \overset{f_T}{\rightarrow} \begin{pmatrix} R_1^* \\ R_2^* \\ \zeta_{Pt} \end{pmatrix}_j \qquad (3)$$

For comparison a shroud contour according to Dejc and Trojanovskij [16] is additionally simulated and evaluated (Ind 02). The shroud contours of the selected optimal individuals Ind 02 and 56 are shown in Fig. 6.

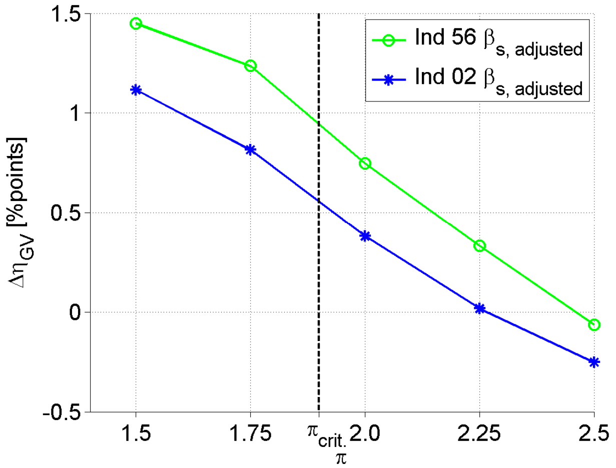

Figure 9. GUIDE VANE EFFICIENCY OVER PRESSURE RATIO RELATIVE TO REFERENCE.

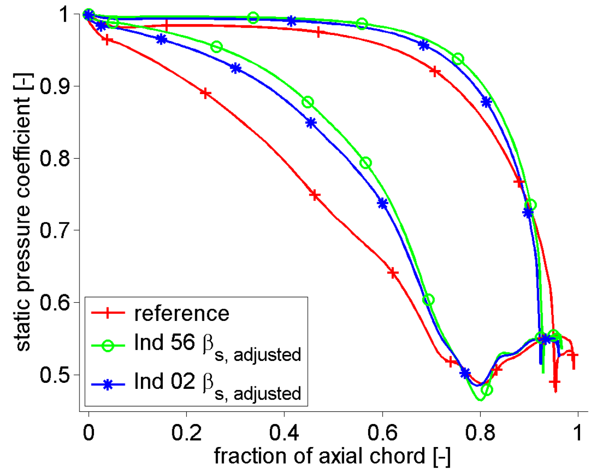

Figure 10. STATIC PRESSURE DISTRIBUTION,SPAN 5%, π = 2.

Table 1. $\Delta\eta_{GV}$ RELATIVE TO REFERENCE AT DESIGN POINT.

	Ind 02	Ind 56
$\Delta\eta_{GV}$ [% points]	0.38	0.75

CFD validation

In order to validate the CFD code, the numerical results of the reference guide vane are compared with measurements of an air turbine test rig. The geometry of the CFD model equates the geometry of the test rig. The aspect ratio of the vane blade is 0.25. The vane pitch ratio equals 0.7. The hub-to-tip ratio is 0.97. The similarity of the Reynolds number is fulfilled for the test rig, the simulation and the real control stage. The boundary conditions at the inlet and outlet are the same for the experiment and the simulation. The midspan pressure distribution on the blade is chosen as comparison between the CFD code and the measurement. Figure 7 shows the distribution at π = 2. Thereby excellent agreement between the experiment and numerical data can be observed. At the suction side in an axial chord range from 0.65 to 0.8 a small difference exists between measurements and CFD. The reason for this is an interaction of the secondary flow and the boundary layer, which is slightly under predicted and damped by the turbulence model, but CFD is generally able to represent this secondary flow phenomenon.

Guide vane simulation results

In a further step the three geometries are investigated at different pressure ratios over the nozzle. The total pressure loss reduction in the guide vane also induces a mass flow rate increase. This causes a shift in the operating condition of the guide vane. To clearly judge the optimization potential the operating point must be kept constant. Therefore the stagger angle (β_S) of the flowpath profiled vanes is reduced at π = 2. According to the baseline design, the stagger angle of the Ind 02 is changed by 3% and the Ind 56 by 2.5%, respectively. Figure 8 shows the mass flow rate over the pressure ratio of all contours with the design and adjusted stagger angle. In the further text only the contours with the adjusted stagger angle are considered.

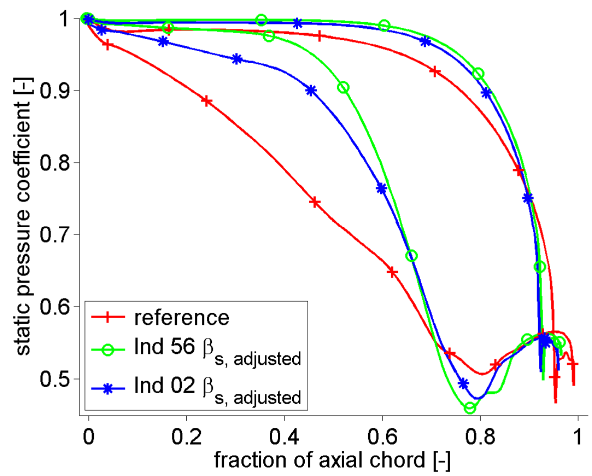

Figure 11. STATIC PRESSURE DISTRIBUTION,SPAN 95%, π = 2.

Table 1 shows the difference of the guide vane efficiency η_{GV} of both optimized shroud profiles in comparison with the reference contour at the design point. η_{GV} is defined as in Eqn. (4). Figure 9 shows $\Delta\eta_{GV}$ relative to the reference contour in the entire operation range. It is noteworthy that the advantage of contouring over the straight contour increases as pressure ratio decreases.

$$\eta_{GV} = \frac{\frac{c_1^2}{2}}{\Delta h_s + \frac{c_0^2}{2}} \tag{4}$$

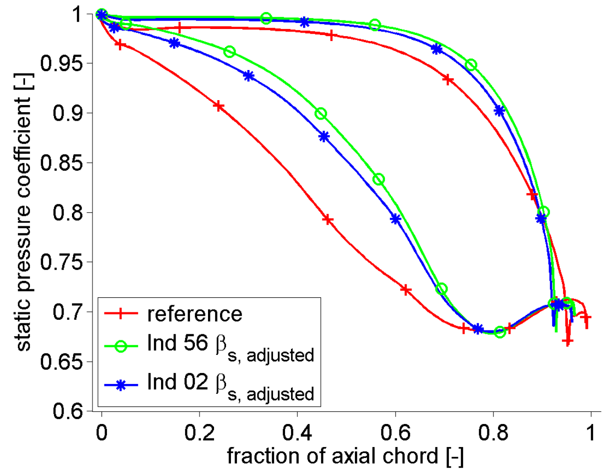

Figure 12. STATIC PRESSURE DISTRIBUTION,SPAN 5%, π =1.5.

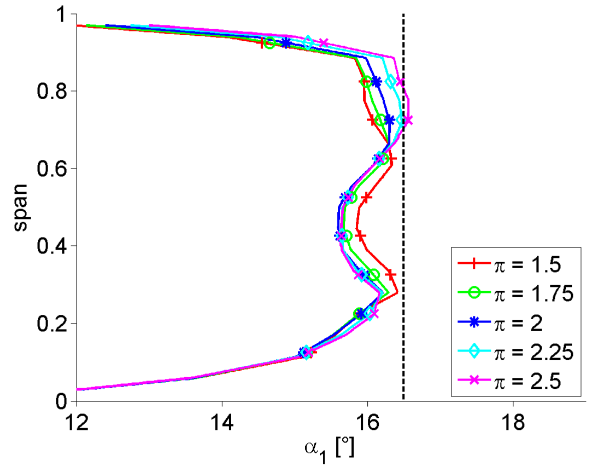

Figure 14. EXIT FLOW ANGLE REFERENCE GEOMETRY.

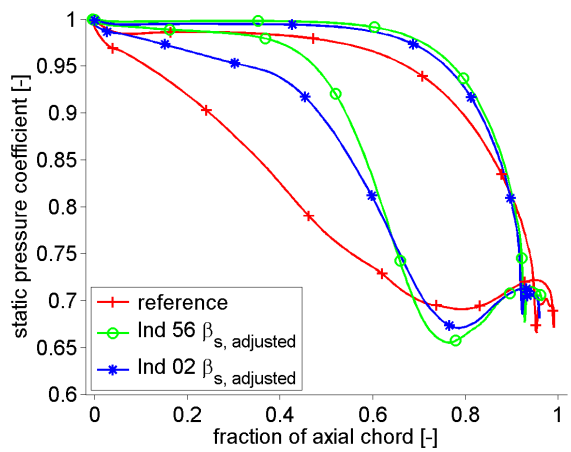

Figure 13. STATIC PRESSURE DISTRIBUTION,SPAN 95%,π =1.5.

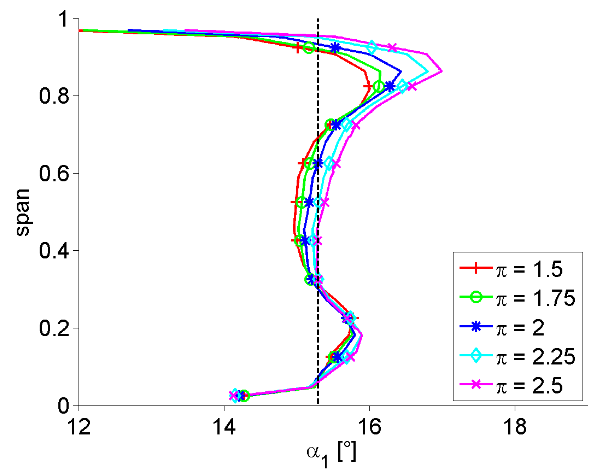

Figure 15. EXIT FLOW ANGLE IND 02 GEOMETRY.

Denton and Xu [17] showed that an end wall profiling reduces the load on the suction side of the nozzle. Figures 10 to 13 depict the static pressure distribution on the blade of all geometries at different span and different pressure ratios.

It can be impressively observed that the flowpath profiling reduces the load at the suction side of the blade profile. This effect especially appears near the end wall. A reduction of the blade load over the upstream half results in a displacement of the high speed flow and acceleration area from the highly curved to the straight section of the blade. This reduces the induction of secondary flows and consequently the boundary layer thickness in this area. This increases the effective flow cross section which results in a slightly higher mass flow rate. The reduction of the secondary flows can be observed at the exit flow angle distribution over the span of the nozzle as well. Figure 14 shows the exit flow angle along the span of the straight nozzle at different pressure ratios. The dashed line marks the geometric exit flow angle of the blade profile. Due to the variation of the stagger angle the geometric exit flow angle also changes. The influence of the passage vortex can be clearly observed at a span of 0.2 and 0.8. Figure 15 and 16 show that flowpath contouring has a strong influence on the shape of the exit flow angle. It can be observed that the passage vortex has been dislocated closer to the end wall. Due to the flowpath profiling also the boundary layer thickness in the nozzle is significantly reduced. Both effects result in a more uniformly shaped exit flow angle profile over the nozzle span at subcritical pressure ratios. It can be mentioned that the influence of the passage vortex on the exit flow angle profile is reduced significantly, too. Over a wider span area the exit flow angle is closer to the geometric exit angle of the blade profile than at the reference geometry. The exit flow angle distribution of the Ind 56 geometry is even more uniform than the one of the Ind 02 geometry. The influence of the passage vortex on the main stream at the mid-span is decreased since it is moved more towards the hub and shroud region. The passage vortex is closer to the end wall at the Ind 56 geometry than at the Ind 02 geometry. Ind 56 and 02 geometries show a weaker passage vortex at the hub than the reference geometry at operating

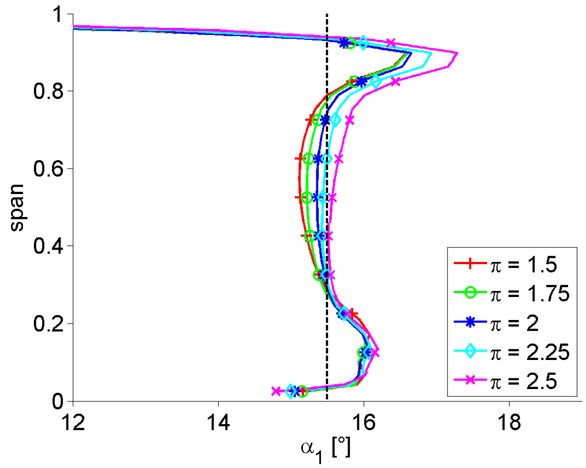

Figure 16. EXIT FLOW ANGLE IND 56 GEOMETRY.

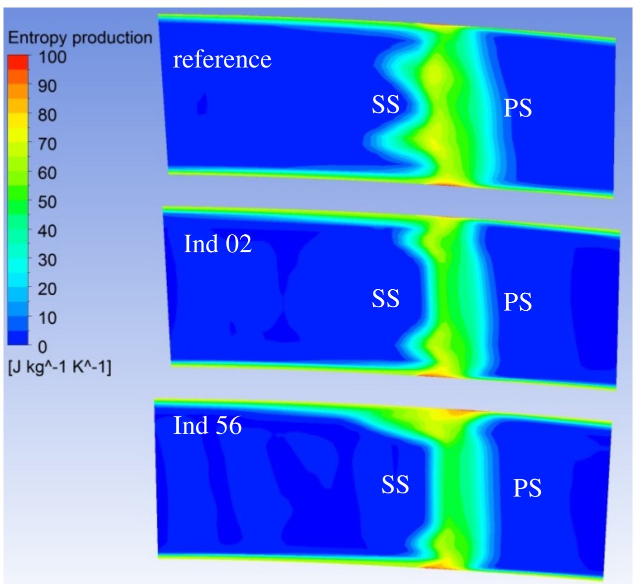

Figure 17. ENTROPY PRODUCTION AT VANE OUTLET

points with subcritical pressure ratio. The passage vortex is moved closer to the shroud wall for Ind 56 than for Ind 02. At supercritical pressure ratios the flowpath profiling induces a more axial flow exit near the shroud. The deviation of the exit flow angle from the geometric angle increases slightly with increasing pressure ratios. The sensitivity to expansion rate changes is slightly increased. This can be explained by the fact that the optimization is undertaken for a fixed pressure ratio. The advantages of the uniform exit flow angle profile exist at all operating conditions. It can be observed at the contour Ind 56 that at pressure ratios of π = 2.25 to 2.5 the influence of the passage vortex close to the shroud increases. At the Ind 02 geometry the influence of the passage vortex increases at pressure ratios of π = 2.25 to 2.5, too. At these pressure ratios the exit flow angle profile of the reference exhibits still a great influence of the passage vortex and the profile is non-uniform along the span of the nozzle.

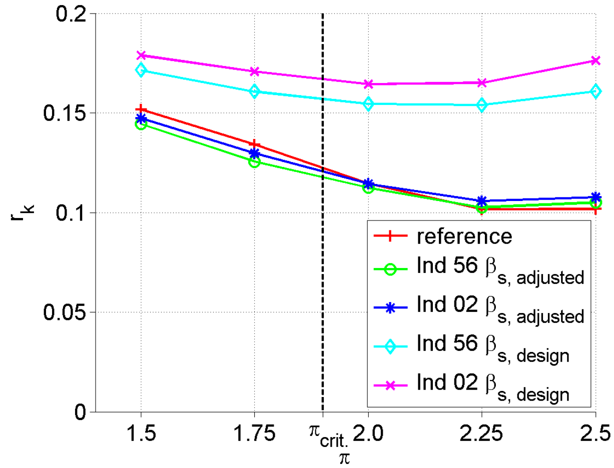

Figure 18. REACTION.

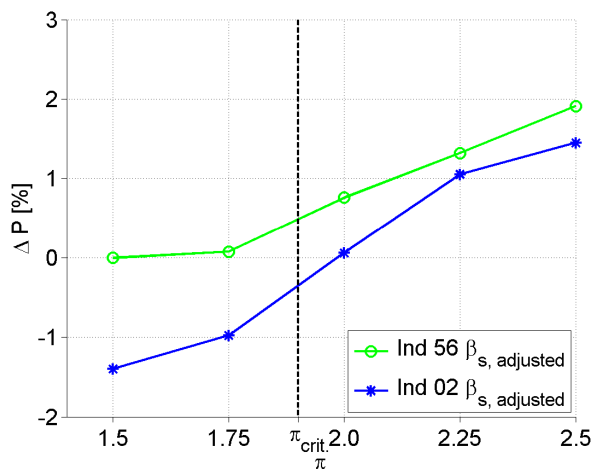

Figure 19. CHANGE OF POWER OUTPUT (ΔP) RELATIVE TO REFERENCE.

Figure 17 shows the entropy production at the guide vane outlet. The contour plots are in good agreement with the results of the exit flow angle. Caused by the passage vortex a large entropy production area can be observed for the reference geometry. Due to flowpath profiling this areas almost vanish. In contrast to this tiny areas of huge entropy production occur in vicinity of the end walls.

Full stage simulation results

At a final step results of the whole control stage have been investigated by CFD. The geometry of the rotor blade has been retained unchanged. The rotor speed is kept constant. The mixing plane interface has been chosen as connection between the rotor and the guide vane. It is a circumferential averaging method between the stator outlet and the rotor inlet. For impulse wheels almost the complete enthalpy drop takes place in the guide vanes. Therefore the stage reaction is around 10 %. As already mentioned, the mass flow rate is increased by flowpath profiling. This leads to a reaction variation of the

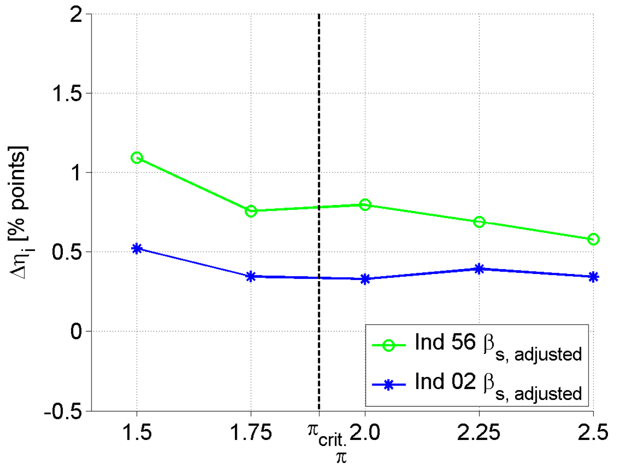

Figure 20. CHANGE OF STAGE EFFICIENCY RELATIVE TO REFERENCE.

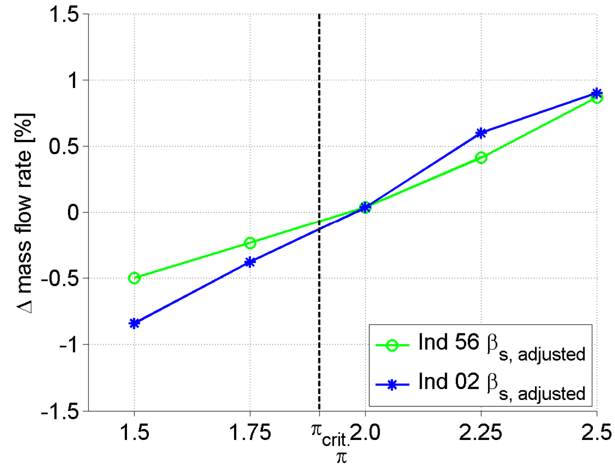

Figure 21. CHANGE OF MASS FLOW RATE RELATIVE TO REFERENCE.

stage as shown in Fig. 18. Due to the modification of the stagger angle the reaction deviation to the reference geometry is minimized.

The variation of the reaction leads to a change of the load distribution between the vane and the rotor. This affects the efficiency of the rotor. In order to prevent this, the reaction of the stage is kept constant for $\pi = 2$ by adapting the stagger angle. The pressure ratio of the following explanations refers to the pressure ratio over the whole stage.

The change of power output in comparison with the reference geometry is shown in Fig. 19. The definition used for the power of the stage is given in Eqn. (5). This definition considers all losses which appear in a stage due to the flow conditions.

$$P = \dot{m}\left(\Delta h + \frac{1}{2}({c_0}^2 - {c_2}^2)\right) \quad (5)$$

Figure 19 illustrates that the Ind 56 contours has a power output benefit over the reference geometry over entire the pressure ratio range. In contrast to this, Ind 02 geometry shows a power decrease for pressure ratios of π = 1.5 to 2.0 in comparison to the reference geometry. The power output benefit of Ind 56 supposes that the stage efficiency is raised due to the flowpath profiling. The efficiency definition used is described in Eqn. (6).

$$\eta_i = \frac{\Delta h + \frac{1}{2}({c_0}^2 - {c_2}^2)}{\Delta h_s + \frac{1}{2}({c_0}^2 - {c_2}^2)} \quad (6)$$

The efficiency advantage of both shroud wall designs shows a more constant behavior over the pressure ratio (Fig. 20) in contrast to the guide vane efficiency η_{GV} (Fig. 9). The decreasing behavior of η_{GV} over the pressure ratio is

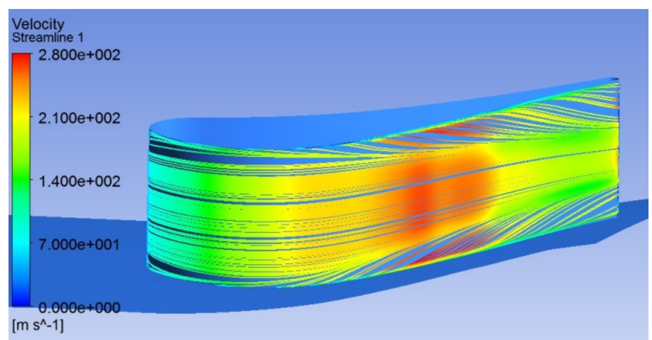

Figure 22. SURFACE STREAMLINES AT SUCTION SIDE REFERENCE GEOMETRY, π = 2.

compensated by an increase of the rotor blade efficiency with the pressure ratio. The Ind 56 geometry has a higher efficiency benefit than Ind 02 geometry at all operation conditions. Figure 21 discloses the relative change of the mass flow rate of the profiled designs in comparison to the reference. It can be observed that the change of the mass flow rate is zero at a π = 2, which can be traced back to the fact that the stagger angle is adjusted for this operating point. The linear behavior of the mass flow rate deviation, explains the offset between the power output and the efficiency increase. This effect is caused by better rotor inflow conditions due to the reduced boundary layer and the smaller passage vortex in the guide vane.

Figures 22 to 24 show surface stream lines at the suction side of the guide vane. Referring to Gbadebo et al. [18] surface streamlines can be used to identify 3D separations and secondary flows. They are infinitesimally close located to the surface. Figures 22 to 24 clearly depict that the exit flow of the Ind 02 and Ind 56 guide vane nozzle is more uniform than of the reference geometry. The extent of the cross section of the undisturbed flow is larger than at the reference geometry. This can be traced back to the effect that the passage vortex is closer to hub and shroud by flowpath profiling. Additionally a slightly stronger local secondary flow can be identified at the shroud of

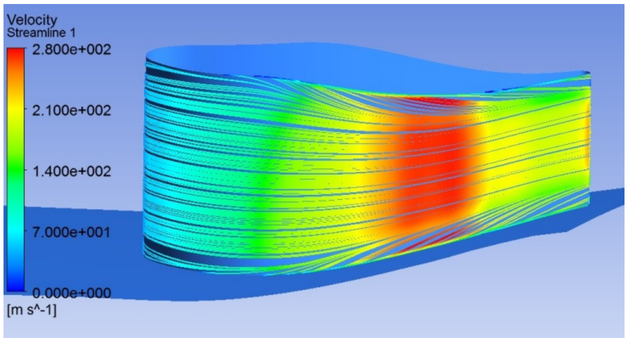

Figure 23. SURFACE STREAMLINES AT SUCTION SIDE IND 02 GEOMETRY, $\pi = 2$.

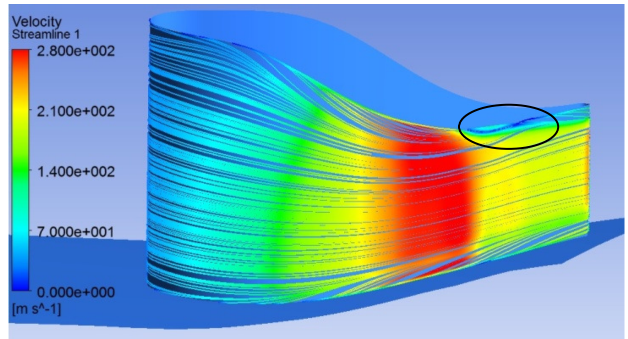

Figure 24. SURFACE STREAMLINES AT SUCTION SIDE IND 56 GEOMETRY, $\pi = 2$.

Ind 56 geometry upstream the trailing edge (see circle in Fig. 24). This effect can also be observed in Fig. 11 at an axial chord of 0.8.

All figures show that both contours have a great efficiency advantage over the reference geometry. But nevertheless the Ind 56 geometry has a greater power output advantage at all pressure ratios in the stage simulation over the Ind 02 geometry. The explanation for this behavior is the higher guide vane efficiency of Ind 56.

CONCLUSION

A new axisymmetric shroud wall contour has been designed for a guide vane of a control stage. This design has been gained by an evolutionary optimization algorithm. This algorithm has been successfully connected to a commercial CFD solver. The objective of the flowpath profiling was the reduction of the total pressure loss and the global secondary flow regimes in the guide vane. By means of flowpath profiling the passage vortex is degraded and dislocated to the end walls at subcritical operating conditions. The consequence of these effects is a more uniform exit flow angle profile along the span of the guide vane. This results in a positive effect in the inlet conditions for the rotor and hence an increase of efficiency and power output of the whole stage. A reduction of the boundary layer thickness in the guide vane is achieved by flowpath profiling. As a result, the mass flow rate is increased. In order to keep the operating conditions constant, the stagger angle is adjusted. This investigation shows that the optimization of the shroud contour is not a simple problem. It demonstrates that an evolutionary algorithm is a suitable optimization method for this problem. However it also discloses that the influence on the rotor has to be taken into account for optimization. In a further step the results of this numerical investigation will be compared with detailed measurements of a rotating air turbine test rig.

ACKNOWLEDGMENTS

The investigations were conducted as part of the joint research program COOREFF-T/COORETEC-turbo in the frame of AG Turbo. The work was supported by the Bundesministerium für Wirtschaft und Technologie (BMWi) as per resolution of the German Federal Parliament under grant number 0327716Q. The authors gratefully acknowledge AG Turbo and MAN Diesel & Turbo SE for their support and permission to publish this paper. The responsibility for the content lies solely with its authors.

REFERENCES

[1] Langston, L., 2001. “Secondary Flows in Axial Turbines – A Review”. Annals of New York Academy Sciences, p. 934.

[2] Sieverding, C. H., 1985. “Recent progress in the understanding of basic aspects of secondary flows in a turbine blade cascade”. *ASME Journal of Engineering Gas Turbines and Power*, **107**(2), pp. 248–252.

[3] Gregory-Smith, F. G., 1997. “Secondary and Tip-Clearance Flows in Axial Turbines”. *VKI LS*, **1997-01**. Von Karman Institute for Fluid Dynamics, Rhode St. Genese, Belgium.

[4] Dejc, M. E., and Zarjankin, A. E., 1960. “Methods of Increasing the Efficiency of Turbine Stages”. *Teploenergetika*, 2, pp. 18–24.

[5] Moustapha, S. H., and Williamson, R. G., 1985. “Investigation of the Effect of two Endwall Contours on the Performance of an Annular Nozzle Cascade”. In Proceedings of AIAA. AIAA-85-1218.

[6] Rose, M. G., 1994. “Non-axisymmetric Endwall Profiling in the HP NGVs of an Axial Flow Gas Turbine”. In Proceedings of ASME Turbo Expo. ASME Paper No. 94-GT-249.

[7] Schnaus, J., and Fottner, L., 1997. “Experimental and Numerical Investigation of the Influence of Endwall Inclination and Contouring on the Flow Field in a Turbine Cascade”. In Proceedings of ISABE. ISABE Paper No. 97-7117.

[8] Duden, A., Raab, I., and Fottner, L., 1999. "Controlling the Secondary Flow in a Turbine Cascade by Three-Dimensional Airfoil Design and Endwall Contouring". *ASME Journal Turbomachinery*, **121**, pp. 191–199.

[9] Harvey, N. W., Rose, M. G., Taylor, M. D., Shapar, S., Hartland, J. C., and Gregory-Smith, D. G., 2000. "Non-axisymmetric Turbine End Wall Design: Part I - Three-Dimensional Linear Design System". *ASME Journal Turbomachinery*, **122**, pp. 278–285.

[10] Hartland, J. C., Gregory-Smith, D. G., Harvey, N. W., and Rose, M. G., 2000. "Nonaxisymmetric Turbine End Wall Design: Part II - Experimental Validation". *ASME Journal Turbomachinery*, **122**, pp. 286–293.

[11] Eymann, S., Foerster, W., Beversdorff, M., Reinmoeller, U., Niehuis, R., and Gier, J., 2002. "Improving 3D flow charakteristics in a multistage LP turbine by means of endwall contouring and airfoil design modification part 1: design and experimental investigation". In Proceedings of ASME Turbo Expo. ASME Paper GT2002-30352.

[12] Rechenberg, I., 1994. *Evolutionsstrategie '94*. Stuttgart : Frommann-Holzboog.

[13] Weicker, K., 2002. *Evolutionaere Algorithmen*. Teubner Verlag.

[14] Moser, N., Joos, F. "Optimization of a Steam Turbine Guide Vane by End Wall Contouring Using Evolutionary Algorithms". In Proceedings of ICEC 2010. Paper ICEC2010-34.

[15] Seber, G. A. F., 1984. *Multivariate Observations*. Wiley.

[16] Dejc, M. E., and Trojanovskij, B. M., 1973. *Untersuchung und Berechung axialer Turbinenstufen.* VEB Verlag Technik.

[17] Denton, J. D., and Xu, L., 1999. "The exploitation of threedimensional flow in turbomachinery design". In Proceedings of the I MECH E Part C Journal of Mechanical Engineering Science, Vol. **213**, pp. 125–137.

[18] Gbadebo, S. A., Cumpsty, N. A., Hynes, T. P., 2004. "Three-Dimensional Separations in Axial Compressors". In Proceedings of ASME Turbo Expo. ASME Paper No. GT2004-53617.